Journal of Oceanography (2019) 75:415–422
https://doi.org/10.1007/s10872-019-00510-z

ORIGINAL ARTICLE

Observations of the Luzon Cold Eddy in the northeastern South China Sea in May 2017

Zhida Huang[1] · Wei Zhuang[2] · Jianyu Hu[2] · Bangqin Huang[3]

Received: 9 November 2018 / Revised: 7 March 2019 / Accepted: 10 March 2019 / Published online: 22 March 2019

Abstract
Combining cruise observations, satellite altimeter and Argos drifter data in the northeastern South China Sea in the spring of 2017, this paper reports a Luzon Cold Eddy (LCE), which originated near the northwestern coast of Luzon Island. Then it migrated northwestward and was sampled by the cruise transect to the southwest of Taiwan Island. In the core of the LCE, the isotherm, isohaline and isopycnal all uplifted by approximately 100 m within the depth range of 150–300 m. The corresponding geostrophic currents were consistent with satellite altimeter results. In addition, a double-index was applied to study the dynamical process for the LCE evolution. The index reflects well the intraseasonal variability of eddies and the Kuroshio pathway in the spring of 2017. During the second half of April, the enhancement of the LCE was regulated by the velocity shear resulting from a large anticyclonic eddy east of the Luzon Strait. Taken together, the results of this study demonstrate a better understanding of the circulation and mesoscale patterns and a potential implication for water mass renewal in the northeastern South China Sea.

Keywords Luzon Cold Eddy · South China Sea · Kuroshio · Double-index · Luzon Strait

1 Introduction

The Luzon Strait (LS) is an important channel for water exchange between the South China Sea (SCS) and the northwest Pacific (NP), as shown in Fig. 1. Much research has been conducted on the complicated dynamic processes related to the Kuroshio and mesoscale eddies near the LS (Jia et al. 2005; Zhuang et al. 2010; Zheng et al. 2011; Nan et al. 2014; Geng et al. 2016, 2018; Zhang et al. 2018). Generally, in winter (summer), the Kuroshio is mainly in a looping (leaping) state in the LS due to a northeasterly (southwesterly) East Asian monsoon and a weaker (stronger) Kuroshio transport (Metzger and Hurlburt 1996; Sheremet 2001; Caruso et al. 2006; Chern et al. 2010; Yuan and Wang 2011; Hsin et al. 2012; Kuo et al. 2017). At the same time, mesoscale eddies may play significant roles in modulating the local circulation system (Chen et al. 2011c; Zheng et al. 2011; Nan et al. 2011; Lien et al. 2014; Huang et al. 2017). Moreover, nonlinear Rossby eddies can propagate into the SCS (Hu et al. 2001, 2012; Zheng et al. 2011), which is supported by both satellite altimeter data and cruise observations. Therefore, in addition to providing a research hotspot near the LS, the Kuroshio-Eddy interaction presents a complex scientific challenge.

Recently, Huang et al. (2016) proposed a double-index (DI) to identify different Kuroshio intrusion paths based on satellite altimeter data, which can well describe Kuroshio-Eddy interaction near the LS. The DI is made up of two sub-indices: the Kuroshio Cold Eddy Index (KCI) and the Kuroshio Warm Eddy Index (KWI). According to the DI, three typical spatial patterns are identified: the Kuroshio warm eddy path (KWEP), the Kuroshio cold eddy path (KCEP), and the leaking path. However, these patterns need further verification by combining cruise observations, satellite data, and so on.

✉ Jianyu Hu
hujy@xmu.edu.cn

[1] State Key Laboratory of Marine Environmental Science, College of the Environment and Ecology, Xiamen University, Xiamen 361102, China

[2] State Key Laboratory of Marine Environmental Science, College of Ocean and Earth Sciences, Xiamen University, Xiamen 361102, China

[3] Fujian Provincial Key Laboratory of Coastal Ecology and Environmental Studies, College of the Environment and Ecology, Xiamen University, Xiamen 361102, China

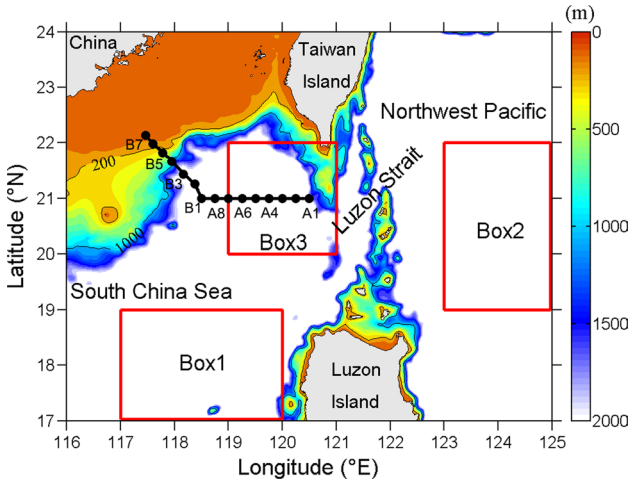

Fig. 1 Distribution of the survey stations (black dots) in the northeastern South China Sea (SCS) in May 2017. The white area represents water depth greater than 2000 m. Box1 (17°N–19°N, 117°E–120°E) and Box2 (19°N–22°N, 123°E–125°E) are selected to plot the mean T–S diagrams for the SCS water and northwest Pacific (NP) water, respectively. Box3 (20°N–22°N, 119°E–121°E) is the integral area for the double-index (DI)

As for the Luzon Cold Eddy (LCE), previous studies have shown that the LCE often appears to the northwest of Luzon Island in winter and spring (Jiang and Hu 2010; Sheu et al. 2010; Sun and Liu 2011; He et al. 2015; Lu et al. 2015; Sun et al. 2015). Based on a variable-grid ocean circulation model, He et al. (2015) reported that the LCE may be weakened by the Kuroshio intrusion. According to satellite altimeter data, Sun and Liu (2011) suggested that Kuroshio velocity shear is important for the LCE formation.

The LCE is one of the most important eddies in the SCS, but it is less explored by cruise measurements. The aim of the present study is to investigate the LCE using cruise observations, satellite altimeter data, and Argos drifter trajectory data in the northeastern SCS, collected in the spring of 2017. The data and methodology are briefly described in Sect. 2. Section 3 presents the major features of the LCE from cruise measurements and investigates dynamics for the LCE evolution according to the satellite altimeter data and using the DI method. Section 4 is the summary and discussion.

2 Data and methodology

During 23–25 May 2017, we carried out a cruise mission conducted onboard the R/V *Yanping No. 2* in the northeastern SCS, and we measured 15 stations using the SBE 917 conductivity-temperature-depth profiler (from the Sea-Bird Electronics), with a station spacing of approximately 0.25° (Fig. 1). This cruise was conducted from Stations A1 to A8 (Transect A) and then northwestward from Stations B1 to B7 (Transect B) for investigating the LCE demonstrated by the satellite altimeter data. The climatologically observed temperature and salinity were derived from the U.S. Navy Generalized Digital Environment Model version 3 (GDEM-V3, http://www.usgodae.org/pub/outgoing/static/ocn/gdem/), with a horizontal grid resolution of 0.25° × 0.25° and a vertical grid of 78 standard layers ranging from the surface to 6600 m (Carnes 2009). We apply this dataset to assess the observed temperature (T) and salinity (S) properties.

Based on the cruise observations, the geostrophic currents ($\vec{U}$) are calculated by the thermal wind relation (Wang et al. 2011), which is defined as:

$$\vec{U} = \frac{g}{f\rho_0}\int_{z_0}^{z}\frac{\partial\rho}{\partial X}\mathrm{d}z \tag{1}$$

where g is the gravitational acceleration, f is the Coriolis parameter, ρ is the potential density, ρ_0 is the reference density (1024 kg m^{-3}), X is the distance (m), and z_0 is the reference level (1000 m). In Eq. 1, $\vec{U}$ is obtained by the central difference method. Along Transects A and B, the positive $\vec{U}$ represents the northward and northeastward components of the geostrophic current, respectively.

The daily merged satellite altimetry data of the spring of 2017 were derived from the Copernicus Marine Environment Monitoring Service (CMEMS; http://marine.copernicus.eu/), with a horizontal resolution of 0.25°. The absolute dynamic topography (ADT) is defined as the sea surface height above the geoid and is obtained by summing the sea-level anomaly (SLA) and the mean dynamic topography. The ADT and the corresponding surface geostrophic currents are used to validate cruise observations. Using the satellite altimeter data, we also explore the dynamic mechanism for the LCE evolution. In addition, the Argos satellite-tracked surface drifters released by the National Oceanic and Atmospheric Administration (NOAA) Atlantic Oceanographic and Meteorological Laboratory (AOML, http://www.aoml.noaa.gov/envids/index.php) are applied to further investigate the LCE. The temporal resolution of the drifter positioning is 1 day (Hansen and Poulain 1996; Zheng et al. 2008).

Following Huang et al. (2016), the DI method is used to investigate spatial patterns of the Kuroshio and mesoscale eddies near the LS. The DI is composed of KWI (I_{kw}) and KCI (I_{kc}) and is defined as follows:

$$I_{\mathrm{kw}} = \iint \mathrm{sign}(-V_{\mathrm{g}})V_{\mathrm{g}}\mathrm{d}A \tag{2}$$

$$I_{\mathrm{kc}} = \iint \mathrm{sign}(V_{\mathrm{g}})V_{\mathrm{g}}\mathrm{d}A \tag{3}$$

where sign() is the sign function:

$$sign(x) = \begin{cases} 1, & x \geq 0 \\ 0, & x < 0 \end{cases}$$

In Eqs. 2 and 3, V_g is the geostrophic vorticity ($\frac{\partial v}{\partial x} - \frac{\partial u}{\partial y}$), where u and v are the surface geostrophic currents. The integral area (A; 20–22°N, 119–121°E) for the DI is shown as Box 3 in Fig. 1. Using standard deviations as the thresholds, the KWEP, KCEP and leaking path are described by Huang et al. (2016). In this study, the KCEP is identified for the spring of 2017.

3 Characteristics and dynamics of the LCE

3.1 Cruise observations

Figure 2 shows sectional distributions of salinity, temperature and potential density along Transects A and B, and the corresponding T–S diagrams are presented in Fig. 3. In the subsurface layer (50–100 m), there were two salinity maximum cores: one was located east of Transect A (Stations A1–A2; 120.25°E–120.50°E), with values greater than 34.9 psu, and the other was located west of Transect B (Stations B5–B6; 117.60°E–117.80°E), with values greater than 34.8 psu (Figs. 2a, d, 3). Below these two high-salinity cores there were two low-salinity cores in the intermediate layer (300–500 m), with values less than 34.4 psu. In the intermediate layer, the minimum salinity value in the LS

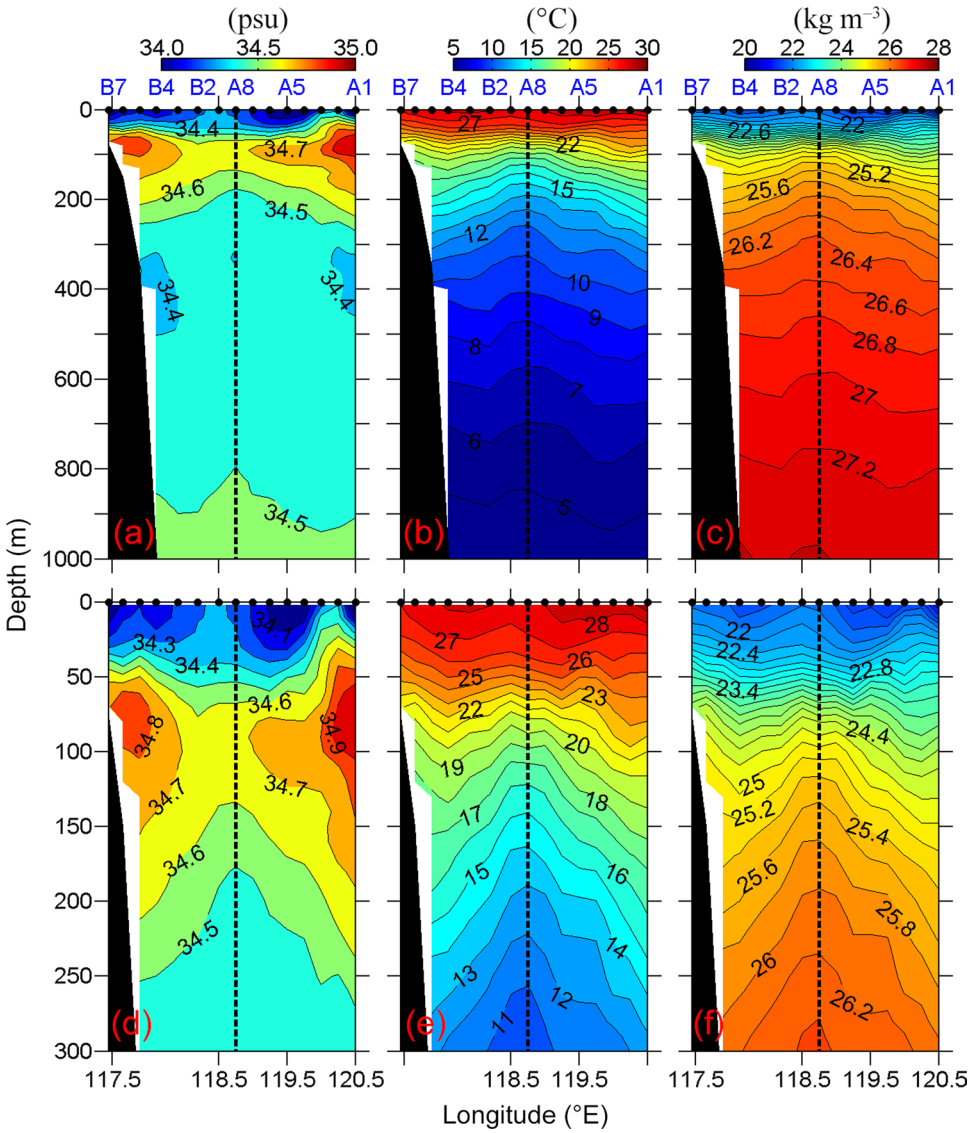

Fig. 2 Distributions of **a** salinity, **b** temperature, and **c** potential density along Transects A and B between 0 and 1000 m. Plots **d**–**f**, are the same except between 0 and 300 m. The black dashed line highlights Station A8, which is near the dividing point of the two transects. The black shades indicate the topography

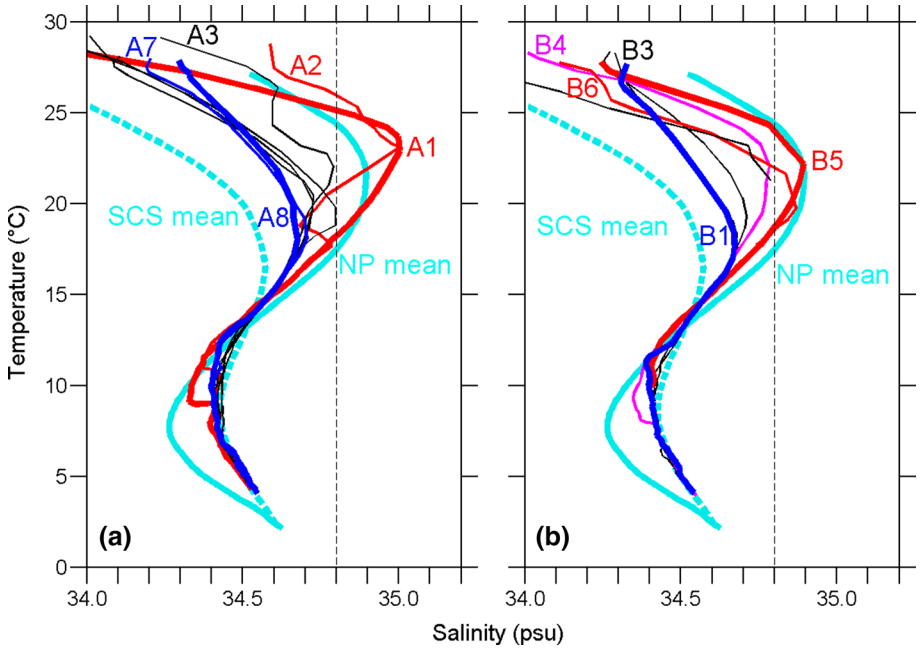

Fig. 3 T–S diagrams at **a** Transect A and **b** Transect B by cruise observations. The dashed and solid light blue lines are the T–S diagrams for the annual mean SCS water (Box1 in Fig. 1) and the annual mean NP water (Box2 in Fig. 1) based on the GDEM-V3 dataset, respectively. The dashed black line highlights a salinity value of 34.8

was consistent with the cruise observation by Chen et al. (2011a). According to the typical T–S diagrams for the NP water and SCS water (Fig. 3), the above salinity distributions demonstrate that the NP water mass appeared not only in the LS, but also in the slope of the northeastern SCS. At Station A8, it is worth noting that the subsurface salinity was between 34.6 and 34.7 psu (Figs. 2d, 3a), which was closer to the climatological SCS water mass. Furthermore, Fig. 2d also shows that the 34.5 and 34.6 psu isohalines between 150 and 300 m uplifted approximately 100 m at Station A8. This uplift phenomenon was more clearly apparent from the 12–16 °C isotherms and 25.4–26.2 kg m^{-3} isopycnals (Fig. 2e, f).

Figure 4 shows the geostrophic currents along Transects A and B, with a reference level of 1000 m. Results over the continental slope (Stations B5–B7) are not taken into account because the water depth is less than 400 m. Along Transect A, the positive (negative) values represent northward (southward) flow, and they denote northeastward (southwestward) flow along Transect B. Overall, northward flow dominates Transect A, whereas southwestward flow dominates Transect B. Near Station A8, the 0 contour line extends from the surface to 1000 m. In the surface layer, the maximum southwestward flow (0.3 m s^{-1}) appears between Stations B1 and B2, and the maximum northward flow (0.3 m s^{-1}) occurs between Stations A6 and A7. This type

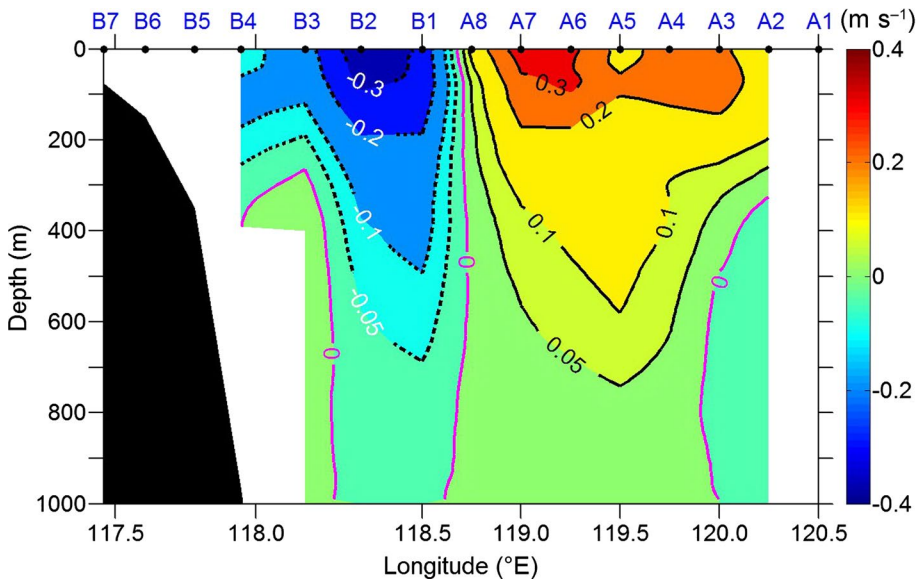

Fig. 4 Distribution of geostrophic currents with a reference level of no motion at 1000 m based on cruise observations. Along Transect A, the positive (negative) values denote northward (southward) flow, whereas they denote northeastward (southwestward) flow along Transect B. The pink lines represent the contour value of 0

of symmetric geostrophic current pattern accords with the major feature of a general cyclonic eddy (CE).

3.2 Results from satellite altimetry products

Figure 5 shows the ADT (cm) distribution and the corresponding surface geostrophic currents (m s^{-1}) during the period of cruise observation. West of the LS, there was a large CE (ADT ≤ 90 cm), with a scale of approximately 200 km. East of the LS, an anticyclonic eddy (AE; ADT ≥ 150 cm) existed east of Taiwan Island, with a scale larger than 200 km. At the same time, the Kuroshio main path was in a leaping path. The AE led to a stronger Kuroshio and provided a favorable condition for CE formation (Sheu et al. 2010; Sun and Liu 2011). Overall, Transect A was located from the east edge of the CE to its core along 21°N, and Transect B was located from the core of the CE to its northwest edge. The surface geostrophic current at Station A8 was close to 0 m s^{-1}, and the southeastward surface geostrophic current component between Stations B1 and B2 and the northward surface geostrophic current component between Stations A6 and A7 were both approximately 0.3 m s^{-1} (Fig. 5). These results are highly consistent with the geostrophic current pattern shown in Fig. 4. Therefore, it is clear that the CE is demonstrated by both satellite altimeter data and cruise observations.

Figure 6 presents the SLA evolution from 18 March to 24 May 2017. Color shadings highlight SLA ≤ –10 cm or SLA ≥ 10 cm. On 18 March, there was a CE northwest of Luzon Island, with a minimum SLA value of approximately –10 cm (Fig. 6a). Compared with 18 March, the CE was slightly enhanced on 30 March, but its core remained unchanged (Fig. 6b). From 30 March to 15 April, the CE moved northward by approximately 1°, accompanied by the minimum SLA decreasing to –15 cm (Fig. 6c). Note that there was a large AE (approximately 200 km) east of the LS on 15 April, with a maximum SLA of 25 cm and its core at 114°E, 20°N (Fig. 6c). Overall, both CE and AE moved northwestward from 15 to 29 April. Notably, the CE was strengthening during this period, with its minimum SLA decreasing to –20 cm (Fig. 6d). On 15 May, the range of the –5 cm SLA contour line shrank, which reflects that the CE was in a decay stage (Fig. 6e). At the same time, the AE moved from the middle LS to east of Taiwan Island. During cruise observations (24 May), the core of the CE was located near Station A8, with a minimum SLA value of approximately –15 cm (Fig. 6f). According to the SLA contour line of –5 cm, the scale of the CE was approximately 200 km, which is consistent with the result of the ADT map shown in Fig. 5. The evolution of the CE provides two important messages: Firstly, the strength of the CE reached a maximum on 29 April when the AE was closest to the Kuroshio's main path, which reflects that CE evolution was related to the AE; Secondly, the CE originated from northwest of Luzon Island, so the CE in this study should be appropriately referred to as LCE (Sun and Liu 2011; He et al. 2015).

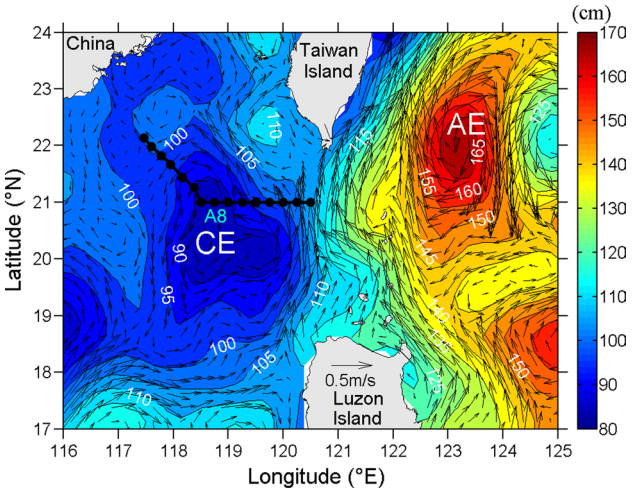

Fig. 5 ADT and corresponding surface geostrophic currents during 23–25 May 2017 derived from satellite altimetry data. The black dots represent survey stations. CE and AE denote cyclonic eddy and anticyclonic eddy, respectively

Figure 7 presents the time series of daily DI (KWI/KCI) from 10 March to 10 June 2017. The dashed green lines highlight the evolution events in Fig. 6. Compared with 18 March, the KCI increased from 1.19 to 2.47×10^5 m^2 s^{-1}, and KWI decreased from –0.67 to -1.79×10^5 m^2 s^{-1} on 30 March (Fig. 7), caused by the development of a small eddy pair with a radius of approximately 50 km in the DI integral area (Fig. 6a, b). Although the KCI was very close to 2.48×10^5 m^2 s^{-1}, it did not satisfy the KCEP criteria. From 30 March to 15 April, the small cyclonic disappeared and the KCI decreased to 0.96×10^5 m^2 s^{-1}. During the second half of April 2017, the LCE moved northward and its core entered the southwestern part of the DI integral area. On 29 April, the corresponding KCI increased to 2.53×10^5 m^2 s^{-1}, a value significantly above the threshold for identifying the KCEP (Fig. 7). From 10 to 24 May, the LCE moved northwestward and decayed, which resulted in the KCI decreasing to 1.57×10^5 m^2 s^{-1}. Therefore, the LCE evolution process could be described by the KCI (Figs. 6, 7). In particular, when the LCE was at its strongest stage (29 April), the KCI satisfied the KCEP criteria. In Fig. 6d, there is a large AE east of the LS, which is consistent with the results of Huang et al. (2016).

3.3 LCE tracked by Argos drifters

Figure 8 shows two Argos drifter trajectories (145,847 and 101934) in the spring of 2017. In Fig. 8, we also plot the LCE trajectory (pink dots) determined by the position of

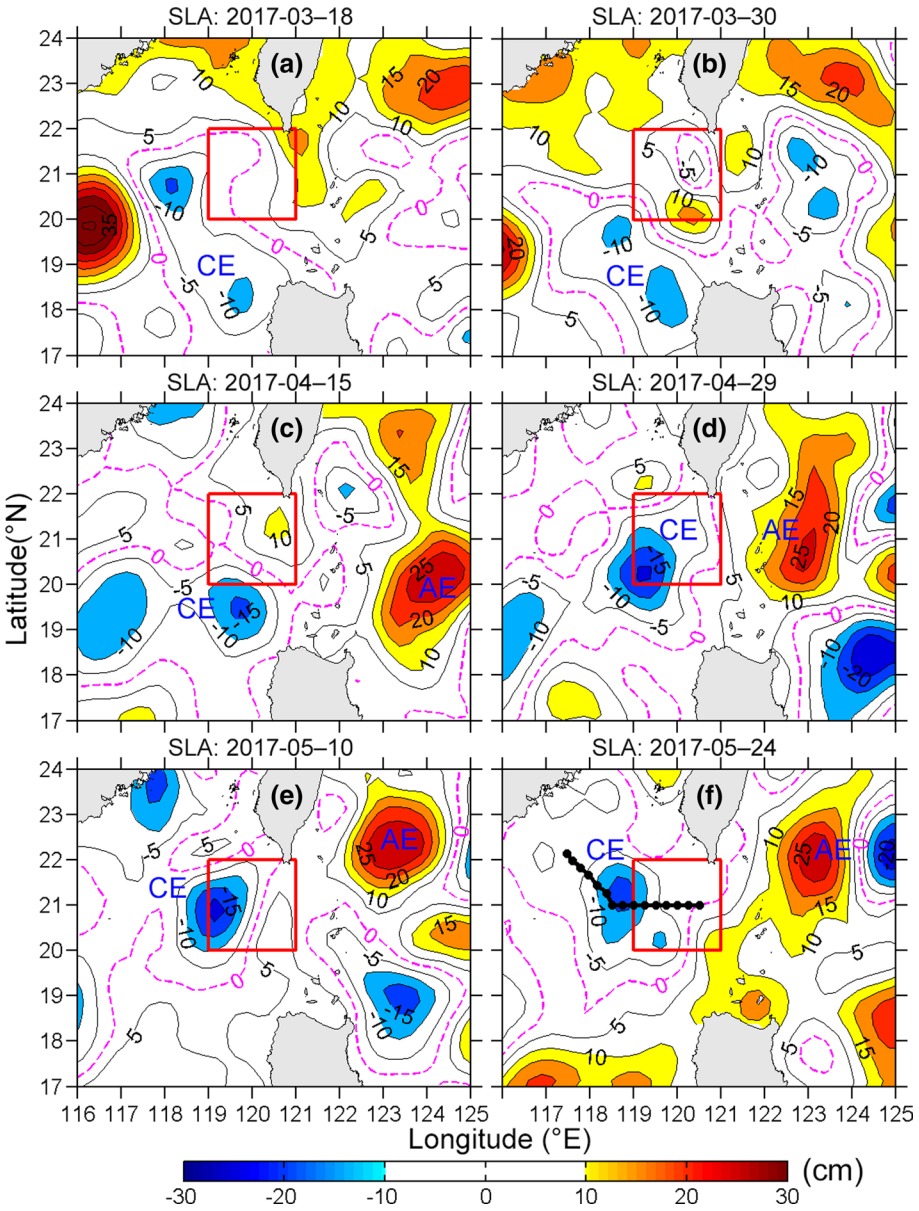

Fig. 6 SLA maps near the Luzon Strait on **a** 18 March, **b** 30 March, **c** 15 April, **d** 29 April, **e** 10 May and **f** 24 May 2017. CE and AE denote cyclonic eddy (Luzon Cold Eddy; LCE) and anticyclonic eddy, respectively. The black dots represent survey stations. Color shadings denote SLA ≤ −10 cm or SLA ≥ 10 cm, and pink dashed lines highlight SLA = 0 cm. The red box is the integral area for the double-index (DI) (color figure online)

minimum SLA according to Fig. 6. Northwest of Luzon Island, the Argo drifter 145,847 (green dots) tracked around the LCE for one cycle during 20–30 March and for another cycle during 2–12 April. During the period of the first cycle, the LCE core estimated from the Argos drifter was approximately 0.25° westward compared with that determined by the SLA map, but it agreed well with that from the ADT maps (not shown). Several dynamical parameters were calculated. For example, the period (T_p) of the drifter rotating around the LCE was approximately 10 days, and the rotational angular velocity ($2\pi/T_p$) was estimated as 0.73×10^{-5} s^{-1}. Moreover, from 13 to 20 April, the LCE was tracked by a semicircular trajectory with a radius of approximately 100 km and its center at 118°E, 19.5°N, which accords with the observation that LCE enhanced and moved northward during this period in the SLA maps (Fig. 6c, d). In addition, during 4–21 May, Argos drifter 101,934 (red dots) moved from northeast of Luzon Island to the LS and then northward to east of Taiwan Island, which matched well with the circulation and mesoscale eddy patterns east of the LS (Fig. 6e, f).

4 Summary and discussion

Using satellite altimeter data, Argos drifter data, and cruise observations from the spring of 2017, this paper analyzes a cold eddy (CE) in the northeastern South China Sea (SCS). The cruise mission was conducted from the east edge of the CE to its core along 21°N, and then turned

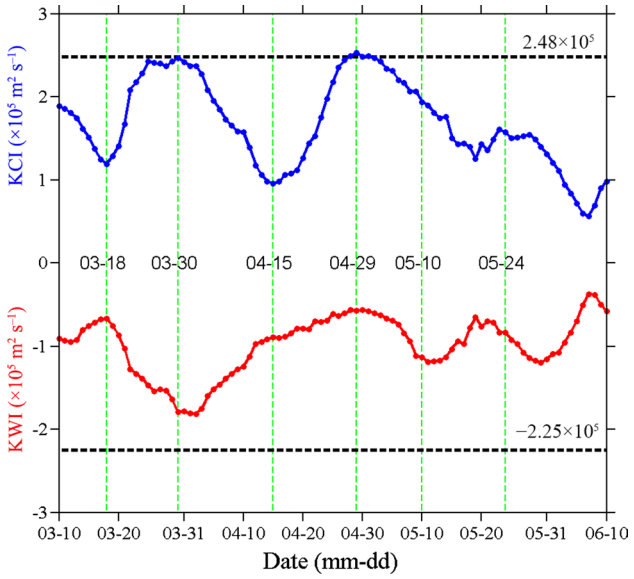

Fig. 7 Time series of the daily KCI (blue) and KWI (red), based on the satellite altimetry data from 10 March to 10 June 2017. The dashed green lines denote the evolution events in Fig. 6. The dashed black lines denote the $\mu+\sigma$ for KCI and $\mu-\sigma$ for KWI from Huang et al. (2016) (color figure online)

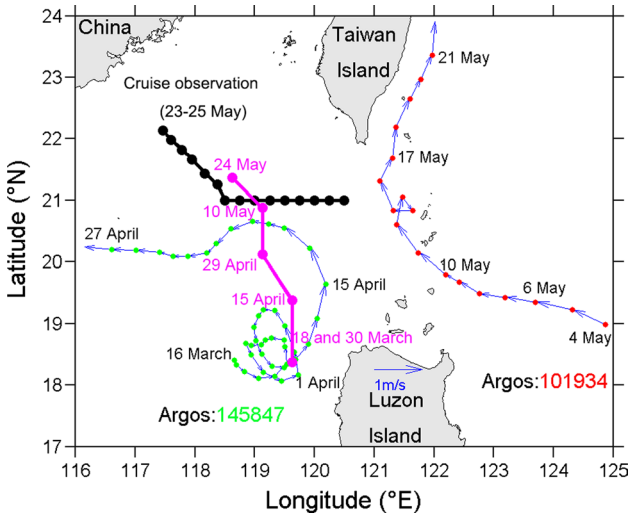

Fig. 8 Two Argos drifter trajectories (145,847 and 101,934) with blue arrows. The green and red dots indicate the daily Argos drifter position. The pink dots denote the LCE trajectory based on Fig. 6. The black dots represent survey stations (color figure online)

northwestward to its edge. Cruise observations showed that the Northwest Pacific (NP) water mass appeared in the east and northwest edges of the CE, and the SCS water mass appeared in the interior of the CE. This phenomenon should be attributed to the CE's rotation or propagation, which transported the NP water from the LS to the slope. In the CE core, the isotherm, isohaline and isopycnal all uplifted by approximately 100 m at the depth range of 150–300 m (Fig. 2), indicating that the CE drove the thermocline shallower, which is different from an anticyclonic eddy (Chen et al. 2011b; Chu et al. 2014). Furthermore, the corresponding geostrophic currents match well with the satellite altimeter results, both of which support the existence of the CE.

According to the evolution processes of satellite altimeter data and Argos drifter trajectories, we find that the CE originated from the so-called Luzon Cold Eddy (LCE; Jiang and Hu 2010; Sheu et al. 2010; Sun and Liu 2011; He et al. 2015). During the period of cruise observations, the LCE was located southwest of Taiwan Island, far away (approximately 300 km) from its formation region northwest of Luzon Island. Following Huang et al. (2016), a double-index (DI) was applied to study the dynamical mechanism for the LCE evolution. The DI is made up of two sub-indices: the Kuroshio Cold Eddy Index (KCI) and the Kuroshio Warm Eddy Index (KWI). Results of the DI indicate that the KCI satisfied the Kuroshio Cold Eddy Path criteria, when the LCE was at its strongest stage on 29 April. During the cruise observations, the LCE moved westward and decayed, which resulted in the KCI decreasing. Furthermore, combining evolution processes of the satellite altimeter data, DI results, and Argos drifter trajectory, this study also reveals that enhancement of the LCE was related to the velocity shear resulting from an anticyclonic eddy (about 200 km) east of the LS. East of the LS, an anticyclonic mesoscale eddy moved westward and collided with the Kuroshio's main path, which led to a stronger Kuroshio and provided a favorable condition for the LCE formation (Sheu et al. 2010; Sun and Liu 2011). By contrast, Chen et al. (2011c) found that a strong CE east of the LS was beneficial to an AE formation in the northeastern SCS, through combining cruise observations carried out in September 2008 and a 1.5-layer model. The above results provide an informative case study on the circulation and mesoscale patterns in the northeastern SCS and could provide better insight into water mass renewal and nutrient dynamics near the LS. In this paper, however, we focused on investigating the LCE observed in May 2017, and more work regarding the annual and interannual variations of the LCE will be done in the future.

Acknowledgements This work was supported by the National Key Research and Development Program of China (No. 2016YFA0601201), the National Basic Research Program of China (No. 2015CB954004), the National Natural Science Foundation of China (Nos. 41776027, 41806011, U1405233), the China Postdoctoral Science Foundation (2018M632577) and the Fundamental Research Funds for the Central Universities (No. 20720160108). The authors would like to thank the CMEMS, GDEM and AOML data centers for their online data, and the NSFC Open Research Cruise (Cruise No. NORC2017-04) for cruise data collection. They would also like to thank the editors and anonymous reviewers for their helpful comments that improved this paper.

References

Carnes MR (2009) Description and evaluation of GDEM-3.0. NRL Rep NRL/MR/7330–09–9165

Caruso MJ, Gawarkiewicz GG, Beardsley RC (2006) Interannual variability of the Kuroshio intrusion in the South China Sea. J Oceanogr 62:559–575

Chen GX, Hou YJ, Chu XQ (2011a) Water exchange and circulation structure near the Luzon Strait in early summer. Chin J Oceanol Limnol 29(2):470–481. https://doi.org/10.1007/s00343-011-0198-0

Chen GX, Hou YJ, Chu XQ (2011b) Mesoscale eddies in the South China Sea: mean properties, spatiotemporal variability, and impact on thermohaline structure. J Geophys Res 116:C06018. https://doi.org/10.1029/2010JC006716

Chen GX, Hu P, Hou YJ, Chu XQ (2011c) Intrusion of the Kuroshio into the South China Sea, in September 2008. J Oceanogr 67:439–448. https://doi.org/10.1007/s10872-011-0047-y

Chern C-S, Jan S, Wang J (2010) Numerical study of mean flow patterns in the South China Sea and the Luzon Strait. Ocean Dyn 60:1047–1059. https://doi.org/10.1007/s10236-010-0305-3

Chu XQ, Xue HJ, Qi YQ, Chen GX, Mao QW, Wang DX, Chai F (2014) An exceptional anticyclonic eddy in the South China Sea in 2010. J Geophys Res 119:881–897. https://doi.org/10.1002/2013JC009314

Geng W, Xie Q, Chen GX, Zu TT, Wang DX (2016) Numerical study on the eddy-mean flow interaction between a cyclonic eddy and Kuroshio. J Oceanogr 72:727–745. https://doi.org/10.1007/s10872-016-0366-0

Geng W, Xie Q, Chen GX, Liu QY, Wang DX (2018) A three-dimensional modeling study on eddy-mean flow interaction between a Gaussian-type anticyclonic eddy and Kuroshio. J Oceanogr 74:23–37. https://doi.org/10.1007/s10872-017-0435-z

Hansen DV, Poulain PM (1996) Quality control and interpolation of WOCE/TOGA drifter data. J Atmos Ocean Technol 13:900–909

He YH, Cai SQ, Wang DX, He JL (2015) A model study of Luzon cold eddies in the northern South China Sea. Deep Sea Res Part I 97:107–123. https://doi.org/10.1016/j.dsr.2014.12.007

Hsin Y-C, Wu C-R, Chao S-Y (2012) An updated examination of the Luzon Strait Transport. J Geophys Res 117:C03022. https://doi.org/10.1029/2011JC007714

Hu JY, Kawamura H, Hong HS, Kobashi F, Wang DX (2001) 3 ~ 6 months variation of sea surface height in the South China Sea and its adjacent ocean. J Oceanogr 57:69–78

Hu JY, Zheng QA, Sun ZY, Tai C-K (2012) Penetration of nonlinear Rossby eddies into the South China Sea evidenced by cruise data. J Geophys Res 117:C03010. https://doi.org/10.1029/2011JC007525

Huang ZD, Liu HL, Hu JY, Lin PF (2016) A double-index method to classify Kuroshio intrusion paths in the Luzon Strait. Adv Atmos Sci 33(6):715–729. https://doi.org/10.1007/s00376-015-5171-y

Huang ZD, Liu HL, Lin PF, Hu JY (2017) Influence of island chains on the Kuroshio intrusion in the Luzon Strait. Adv Atmos Sci 34(3):397–410. https://doi.org/10.1007/s00376-016-6159-y

Jia YL, Liu QY, Liu W (2005) Primary study of the mechanism of eddy shedding from the Kuroshio bend in Luzon Strait. J Oceanogr 61:1017–1027

Jiang LH, Hu JY (2010) Seasonal variability of the Luzon cold eddy and its relation with wind stress. J Oceanogr of Taiwan Strait 29(1):114–121 (in Chinese with English abstract)

Kuo Y-C, Chern C-S, Zheng Z-W (2017) Numerical study on the interactions between the Kuroshio current in the Luzon Strait and a mesoscale eddy. Ocean Dyn 67:369–381. https://doi.org/10.1007/s10236-017-1038-3

Lien R-C, Ma B, Cheng Y-H, Ho C-R, Qiu B, Lee CM, Chang M-H (2014) Modulation of Kuroshio transport by mesoscale eddies at the Luzon Strait entrance. J Geophys Res Oceans 119:2129–2142. https://doi.org/10.1002/2013JC009548

Lu WF, Yan X-H, Jiang YW (2015) Winter bloom and associated upwelling northwest of the Luzon Island. J Geophys Res Oceans 120:533–546. https://doi.org/10.1002/2014JC010218

Metzger EJ, Hurlburt HE (1996) Coupled dynamics of the South China Sea, Sulu Sea, and the Pacific Ocean. J Geophys Res 101(C5):12331–12352

Nan F, Xue HJ, Xiu P, Chai F, Shi MC, Guo PF (2011) Oceanic eddy formation and propagation southwest of Taiwan. J Geophys Res 116:C12045. https://doi.org/10.1029/2011JC007386

Nan F, Xue HJ, Yu F (2014) Kuroshio intrusion into the South China Sea: a review. Prog Oceanogr 137:314–333

Sheremet VA (2001) Hysteresis of a western boundary current leaping across a gap. J Phys Oceanogr 31:1247–1259

Sheu W-J, Wu C-R, Oey L-Y (2010) Blocking and westward passage of eddies in the Luzon Strait. Deep Sea Res Part II 57:1783–1791. https://doi.org/10.1016/j.dsr2.2010.04.004

Sun CX, Liu QY (2011) Double eddy structure of the winter Luzon Cold Eddy based on satellite altimeter data. J Tropical Oceanogr 30(3):9–15 (in Chinese with English abstract)

Sun RL, Zheng L, Chen CL, Yan YW (2015) Interannual variability of thermal front west of Luzon Island in boreal winter. Acta Oceanol Sin 34(11):102–108. https://doi.org/10.1007/s13131-015-0753-1

Wang GH, Xie S-P, Qu TD, Huang RX (2011) Deep South China Sea circulation. Geophys Res Lett 38:L05601. https://doi.org/10.1029/2010GL046626

Yuan DL, Wang Z (2011) Hysteresis and dynamics of a western boundary current flowing by a gap forced by impingement of mesoscale eddies. J Phys Oceanogr 41:878–888. https://doi.org/10.1175/2010JPO4489.1

Zhang WZ, Ni QB, Xue HJ (2018) Composite eddy structures on both sides of the Luzon Strait and influence factors. Ocean Dyn 120:1–15. https://doi.org/10.1007/s10236-018-1207-z

Zheng QA, Lin H, Meng JM, Hu XM, Song YT, Zhang YZ, Li CY (2008) Sub-mesoscale ocean vortex trains in the Luzon Strait. J Geophys Res 113:C04032. https://doi.org/10.1029/2007JC004362

Zheng QA, Tai C-K, Hu JY, Lin HY, Zhang R-H, Su F-C, Yang XF (2011) Satellite altimeter observations of nonlinear Rossby eddy-Kuroshio interaction at the Luzon Strait. J Oceanogr 67:365–376. https://doi.org/10.1007/s10872-011-0035-2

Zhuang W, Xie S-P, Wang DX, Taguchi B, Aiki H, Sasaki H (2010) Intraseasonal variability in sea surface height over the South China Sea. J Geophys Res 115:C04010. https://doi.org/10.1029/2009JC005647